ACS Partner Journal

CHEM & BIO ENGINEERING

Editors' Choice

Open Access

pubs.acs.org/ChemBioEng

Article

Alumina Incorporation in Self-Supported Poly(ethylenimine) Sorbents for Direct Air Capture

Pavithra Narayanan, Pranav Guntupalli, Ryan P. Lively,* and Christopher W. Jones*

Cite This: *Chem Bio Eng.* 2024, 1, 157−170

Read Online

ACCESS | Metrics & More | Article Recommendations | Supporting Information

ABSTRACT: Self-supported branched poly(ethylenimine) scaffolds with ordered macropores are synthesized with and without Al_2O_3 powder additive by cross-linking poly(ethylenimine) (PEI) with poly(ethylene glycol) diglycidyl ether (PEGDGE) at −196 °C. The scaffolds' CO_2 uptake performance is compared with a conventional sorbent, i.e., PEI impregnated on an Al_2O_3 support. PEI scaffolds with Al_2O_3 additive show narrow pore size distribution and thinner pore walls than alumina-free materials, facilitating higher CO_2 uptake at conditions relevant to direct air capture. The PEI scaffold containing 6.5 wt % Al_2O_3 had the highest CO_2 uptake of 1.23 mmol/g of sorbent under 50% RH 400 ppm of CO_2 conditions. *In situ* DRIFT spectroscopy and temperature-programmed desorption experiments show a significant CO_2 uptake contribution via physisorption as well as carbamic acid formation, with lower CO_2 binding energies in PEI scaffolds relative to conventional PEI sorbents, likely a result of a lower population of primary amines due to the amine cross-linking reactions during scaffold synthesis. The PEI scaffold containing 6.5 wt % Al_2O_3 is estimated to have the lowest desorption energy penalty under humid conditions, 4.6 GJ/t_{CO2}, among the sorbents studied.

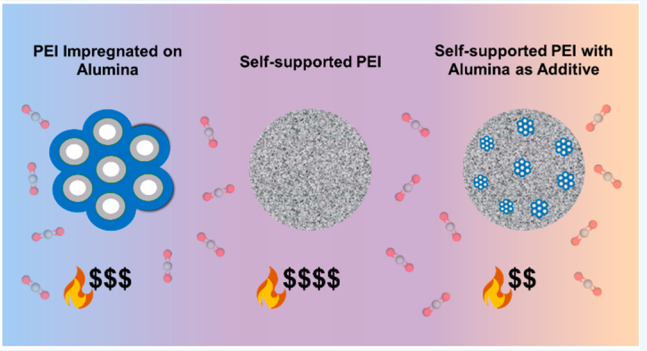

KEYWORDS: *CO_2 capture, direct air capture, solid contactor, amine adsorbent, thermal energy of desorption*

INTRODUCTION

It has been over two decades since the use of direct air capture (DAC) for climate change mitigation was first introduced by Lackner in 1999.[1] There have been many experimental studies published since then to develop materials to cater to DAC,[2−10] and to understand the feasibility of existing materials in the post-combustion flue gas capture technology repository toward DAC.[11−20] Focus on DAC has grown exponentially over the last decade, with a myriad of commercial ventures and start-ups entering the field. According to the International Energy Agency (IEA), there are a total of twenty-seven DAC plants commissioned worldwide so far with a total capturing capacity of ∼0.01 Mt CO_2/year.[21] This is still far from the necessary target, given that annual emissions for the year 2022 were estimated by the IEA to be 36.8 Gt CO_2/year.[22] Two key bottlenecks are leading to this massive gap between the target and current progress: (1) the ultradilute concentration of CO_2 in the air, giving very minimal driving force to aid the capture technology; (2) the cost associated with the DAC infrastructure, its energy use, CO_2 storage, and related factors that make it challenging for the budding technology companies in the initial phase. The energy requirement can be a significant portion of the operating cost associated with DAC. Several estimates have been made for DAC, ranging from ∼1 to 10 GJ/t_{CO2}, with an intrinsic thermodynamic penalty being ∼0.44 GJ/t_{CO2}.[23] Leonzio et al. have determined the cost associated with the energy requirement to be about 51% of the OPEX estimate in amine-functionalized sorbents.[24]

To enable a cost-efficient DAC system, several recent reports have focused on developing solid, structured contactors such as monoliths[4,5,25−29] fibers,[8,30−35] and laminates[36,37] for carbon capture, with a focus on practical scalability. These contactors come with the advantages of modularity, which makes them scalable; they have superior mass transfer properties, provide an opportunity for better heat management, and have the ability to better deal with adsorbent degradation. Most of the contactors contain amine functionalities due to amines' suitability as sorbents in ultra-dilute CO_2 capture and a support structure to increase the accessibility of the amine sites. Among them, monoliths have the advantage of the least pressure drop across a wide range of superficial velocities.[38] This work focuses on developing self-supported poly(ethylenimine) (PEI) contactors with minimal Al_2O_3

Received: October 29, 2023
Revised: January 17, 2024
Accepted: January 28, 2024
Published: February 20, 2024

additive using ice-templating to potentially reduce the support material's dead weight and associated energy penalty.

Ice-templating is a technique where temperature, non-solvent, or reaction-induced phase separation occurs with simultaneous nucleation and growth of ice crystals at sub-ambient temperature, leaving behind porosity when the ice crystals are thawed. The frozen phase in the process consists mainly of ice crystals, while the nonfrozen phase consists of other components in the reaction mixture (in this case, polymer, crosslinker, and additive, if present). Since ice-templating involves the expulsion and concentration of non-aqueous components in the non-frozen phase, it is also called cryo-concentration. It has been used since 1981[39] to induce porosity in various materials, including polymers,[40−42] metals,[43,44] ceramics,[45] and carbon materials.[46] In this work, PEI undergoes a cross-linking reaction with poly(ethylene glycol) diglycidyl ether (PEGDGE) to undergo phase separation. Ice-templating has gained widespread attention over the years owing to the tunability of the macropore size and distribution, depending on parameters such as the temperature of cross-linking, rate of freezing, and direction of freezing.[47] Further, the method has the advantage of a simple single-pot synthesis with water as a green solvent. In two previous studies, self-supported PEI sorbents were synthesized, focusing on post-combustion flue gas capture and understanding the effect of associated acid gas impurity on the sorbent performance.[48,49]

Several studies have shown that the support material used in the supported amine sorbents can affect the performance of the sorbent. Maresz et al. demonstrated that a hierarchically structured monolithic support with a thin active layer offered better accessibility to amine sites and, hence, had better CO_2 uptake kinetics. Rim et al. showed that the nature of support material and, thereby, the interaction of amines with the support material plays a crucial role in the reaction mechanism of amine with CO_2.[50] Since the CO_2−amine interaction could be strong or weak depending on the interaction of the latter with the support, this could be tuned to suit the desired desorption conditions. While the self-supported PEI sorbents or PEI scaffolds synthesized in this work do not have a support material to guide the amine-CO_2 interaction, the presence of an Al_2O_3 additive in the sorbent is hypothesized to affect the nature of the amine−CO_2 interaction, apart from affecting the morphology of the scaffold during the ice-templating. A PEI scaffold with Al_2O_3 additives can be thought of as a continuous polymer matrix with interspersed "support", i.e., amine groups in the scaffold compete for interaction with the limited Al_2O_3 surface. To date, the PEI/Al_2O_3 systems studied so far in the literature have a semicontinuous Al_2O_3 matrix, with PEI coated on them and the Al_2O_3 surface hydroxyl groups competing for the limited accessible amine sites.

Here, alumina particles are incorporated into ice-templated cross-linked PEI scaffolds, and the new materials are compared to conventional PEI-impregnated Al_2O_3 supports (PEI@Al_2O_3) and alumina-free cross-linked scaffolds reported previously.[48,51]

MATERIALS AND METHODS

The following chemicals were purchased from Sigma-Aldrich and used without further purification: 50 wt % branched poly(ethylenimine) (b-PEI, Mw 750 000 by light scattering (LS) and Mn 60 000 by gel permeation chromatography (GPC)) in aqueous solution (referred to in this work as PEI60k), branched poly(ethylenimine) (b-PEI 800, Mw 800 and Mn 600) (referred to in this work as PEI800), poly(ethylene glycol) diglycidyl ether (PEGDGE, Mn 500), and methanol (99.8% ACS grade). The primary, secondary, and tertiary amine ratio (1°/2°/3°) of b-PEI (Mn 60 000 by GPC) was determined by inverse gated ^{13}C NMR to be 37/31/32. The NMR spectra are shown in Figure S1. This ratio agrees with that of similar b-PEI in the literature.[52] Catalox HTa γ-Al_2O_3 was obtained from Sasol. Washing solvents such as methanol, hexane, and acetone were purchased from VWR and used directly. Nitrogen (UHP), helium (UHP), ultra zero grade air, and specialty gas mixtures of 400 ppm of CO_2 in helium and nitrogen were purchased from Airgas Inc.

Synthesis of Benchmark Material. This study used low molecular weight b-PEI (PEI800) that is physically impregnated on γ-Al_2O_3 as a benchmark material. PEI was impregnated on γ-Al_2O_3 by a wet impregnation method.[51,53] Briefly, 1 g of γ-Al_2O_3 dried in a convection oven at 105 °C for at least 48 h was dispersed in 15 mL of methanol (99.8%, ACS reagent). A targeted amount of b-PEI 800 (depending on the desired loading) was separately dissolved in 20 mL of methanol. The two mixtures were stirred separately at room temperature at 300 rpm for at least 1 h before mixing dropwise by adding the PEI/methanol mixture to the γ-Al_2O_3 dispersion. The mixture was stirred for 24 h at room temperature. Methanol was removed in a rotary evaporator at 163.5 Torr, with a water bath at 50 °C. This step was followed by drying the sample at 100 °C overnight under a high vacuum of 12 mTorr. The samples prepared with the above method are named XX_PEI@Al_2O_3, with "XX" being the wt % of PEI impregnated on the γ-Al_2O_3 support. The wt % of PEI impregnated on the γ-Al_2O_3 support was determined from thermogravimetric analysis, the details of which are included in the Characterization section below. The names γ-Al_2O_3 and Al_2O_3 are used interchangeably from here on.

Synthesis of Self-Supported PEI. Self-supported PEI was synthesized by cross-linking high molecular weight b-PEI (PEI60k) at subambient temperatures using ice-templating, similar to the procedure followed in our previous works.[48,49] The method was proposed elsewhere by Chatterjee et al.[41] The cross-linking reaction involves aminolytic ring-opening of epoxide, as shown in Scheme 1.

Scheme 1. S_N2 Aminolytic Ring-Opening of Epoxide between PEI and PEGDGE

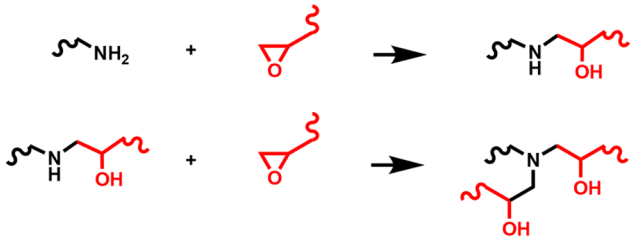

This work used small amounts of γ-Al_2O_3 as an additive in the cross-linking reaction. Briefly, a 50 wt % b-PEI (Mn 60 000 by GPC and Mw 750 000 by LS) solution obtained from Sigma-Aldrich was diluted in DI water to obtain a 9.09 wt % b-PEI stock solution. Then, 1600 μL of the above-mentioned b-PEI stock solution containing 160 mg of b-PEI was taken in a 2-dram glass vial. The required amount of γ-Al_2O_3 (0, 10, 20, 40, 60 mg) was added and mixed in a vortex mixer at 500 rpm for at least 10 min. This resulted in a homogeneous suspension of γ-Al_2O_3 in the b-PEI stock solution. Then, 200 μL of PEGDGE was added to the suspension in the glass vial and mixed in a vortex mixer for 5 s. The mass ratio of b-PEI to PEGDGE in the vial was 7:10. This ratio was used in our previous study and was found to have maximum CO_2 adsorption capacity from a feed gas of 10% CO_2 balanced by N_2.[48] Also, the mass ratio of γ-Al_2O_3 to b-PEI in the mixture ranged between 0 and 3/8, depending on the amount of γ-Al_2O_3 added. The suspension was immediately frozen at −196 °C (liquid nitrogen bath) for 2 min before being placed in a freezer at −10 °C for 2 days. The sample was then thawed at room temperature

https://doi.org/10.1021/cbe.3c00079
Chem Bio Eng. 2024, 1, 157−170

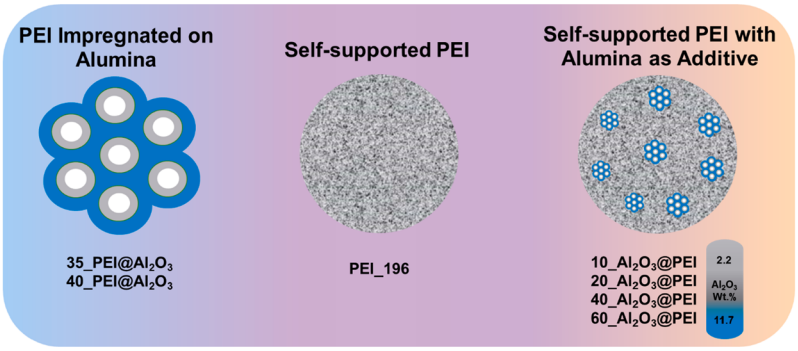

Figure 1. Synthesized sorbents: PEI (gray) impregnated on Al_2O_3 (blue), PEI scaffold without and with Al_2O_3 additive.

after adding 2 mL of methanol to the glass vial. Once at room temperature, methanol and any water from ice melting in the vial were drained, and the scaffold was removed after carefully breaking the vial. The obtained scaffold was sequentially washed in methanol and hexane before drying it in a high vacuum (~12 mTorr) overnight at room temperature. The scaffolds were named PEI_196 when no γ-Al_2O_3 was used and YY_Al_2O_3@PEI when γ-Al_2O_3 was used, with "YY" indicating the amount in mg of γ-Al_2O_3 used. It should be noted that YY, ranging from 10 to 60, is the absolute amount of γ-Al_2O_3 in mg added during the cross-linking and not the amount of γ-Al_2O_3 retained in the sample. The latter was determined from thermogravimetric analysis, the details of which are included in the Characterization section.

Figure 1 shows a representation of the synthesized sorbents-PEI impregnated on Al_2O_3 support, self-supported PEI scaffold, and self-supported PEI scaffold with alumina additive.

Characterization. The actual loading of Al_2O_3 in PEI@Al_2O_3 and Al_2O_3@PEI was determined from combustion thermogravimetric analysis (TGA) experiments conducted in T.A. Instruments TGA550. For each experiment, 10 (± 0.3 mg) of the sample was loaded in the sample pan, and the furnace temperature was increased from room temperature to 125 °C under 100 mL[STP]/min of N_2 and then to 700 °C under 100 mL[STP]/min of ultra zero grade air. The ramp rate for both the steps was 10 °C/min. Mass loss below 125 °C indicated a loss of water and other volatile species, while the loss between 125 and 700 °C indicated the combustion of the organic portion of the adsorbent. The remaining mass at 700 °C was associated with the inorganic alumina loading, which was validated by minimal weight loss exhibited by the neat Al_2O_3 up to 700°C.

The specific surface area, pore size distribution, and pore volumes of γ-Al_2O_3 and PEI@Al_2O_3 were estimated from nitrogen physisorption measurements conducted in Micromeritics Tristar II 3020 apparatus at 77 K. The samples were degassed under a 36 Torr vacuum at 110 °C for 12 h prior to the physisorption measurements. The measurement was performed across a P/P_0 range of 0.061 to 0.998.

Scanning electron microscopy (SEM) was used to study the morphology of the cross-linked PEI scaffolds and to obtain the alumina particle size. A lateral or cross-sectional slice of the scaffold was mounted on an SEM stub using carbon tape. The alumina particles were dispersed in methanol, and the homogenous suspension obtained after mixing in a vortex mixer for 30 min at 500 rpm was dropped onto an SEM stub with carbon tape and air-dried to prevent aggregation and minimize overlapping of particles. Images were captured at an accelerating voltage of 3 kV in Zeiss Ultra60 FE-SEM. The average pore length and wall thickness of cross-linked scaffolds and the particle size of alumina were estimated using open-source software *ImageJ* v1.53e. SEM images obtained were changed into binary form, and Analyze Particles, a built-in function in the software, was used to estimate the pore size distributions. The Feret diameter was used to estimate the length of individual pores. It is defined as the distance between two parallel planes restricting the object perpendicular to the direction of the pore.[57] Since it is similar to the size measurement in a caliper, it is also called the caliper diameter. Further, the pore wall thickness distribution was estimated using an *ImageJ* image processing plugin called Nearest Distance (ND), available in the literature.[58] The coordination number for the pores was chosen as four, based on the average number of pores surrounding any given pore in the SEM images. At least 150 pores and particles, respectively, were considered to obtain the size distributions. Furthermore, the sample's aluminum and oxygen atom distributions were assessed using energy dispersive spectroscopy (EDS) attached to the Zeiss Ultra60 FE-SEM instrument at an accelerating voltage of 5 kV. The voltage was chosen to have more than twice the highest excitation energy among the elements present.

Elemental compositions (C, H, and N) of the samples were measured by combustion at Atlantic Microlab, Norcross, GA. This elemental composition was used to determine the amine efficiency of the sorbents (mol CO_2 sorbed/mol N in sorbent).

Water Uptake Measurements. The water uptake on the PEI@Al_2O_3, PEI_196, 40_Al_2O_3@PEI, and 60_Al_2O_3@PEI sorbents was measured gravimetrically and volumetrically to include a wide range of humidity (~0 to ~98% R.H.) at three different temperatures (30, 40, and 50 °C) using a VTI SA+ and Anton Paar VStar, respectively. For the volumetric measurements, about 100 mg of the sample was pre-treated *in situ* under 0.07 Torr vacuum at 60 °C for 12 h. The manifold was heated to 110 °C to prevent the condensation of water vapor. The gravimetric method used activation at 100 °C under nitrogen flow for 12 h. About 30 mg of sample was used in the measurements taken in VTI SA+.

CO_2 Adsorption Measurements. Dry CO_2 uptake for the samples was measured by thermogravimetric analysis (T.A. Instruments Q500). In a typical experiment, 17 mg (± 0.3 mg) of the sample was first activated in pure N_2 at 100 °C for 3 h. Adsorption was then carried out with a feed gas of 400 ppm of CO_2 balanced by N_2 at 30 °C for 720 min. The specific CO_2 concentration used herein was relevant to direct air capture. Humid CO_2 uptake was measured in a custom-modified thermogravimetric analysis (T.A. Instruments Q500) equipped with a dew point generator, as shown in Figure S2. The procedure was similar to that adopted in the dry CO_2 uptake measurements. However, the adsorption segment was preceded by a pre-saturation segment in a humid nitrogen stream for 200 min. A relative humidity of 50% was achieved using a LiCOR dew point generator. A minimum of 3 °C difference was needed between the dew point temperature set in the dew point generator and the ambient air temperature for safe operation without water condensation in the gas lines. Hence, for a given ambient temperature of ~22 °C, 50% RH was the maximum attainable relative humidity in the instrument. The mass uptake during the presaturation stage was also used to determine the water uptake of the sorbents at that temperature and humidity.

Temperature-Programmed Desorption. CO_2/H_2O temperature-programmed desorption (TPD) experiments were conducted to probe the materials' behavior under dry and humid (50% RH) 400 ppm of CO_2 conditions. Before desorption, the steps of activation, presaturation (for humid conditions), and adsorption were carried out

https://doi.org/10.1021/cbe.3c00079
Chem Bio Eng. 2024, 1, 157−170

following the procedure mentioned earlier for CO_2 adsorption capacity measurements. The desorption step consists of three stages: (i) Purging with N_2 at adsorption temperature (30 °C) for 3 h, (ii) purging with N_2 with a temperature ramp of 0.5 °C from 30 to 100 °C, and (iii) purging with N_2 at 100 °C for 1 h. A nitrogen flow rate of 90 mL[STP]/min was used.

***In Situ* Diffuse Reflectance Infrared Fourier Transform Spectroscopy.** *In situ* FT-IR spectroscopy was performed using a custom-built gas dosing system and a Harrick Praying Mantis diffuse reflectance accessory in a Nicolet iS10 I.R. spectrometer from Thermo Scientific. A schematic diagram of the setup is shown in Figure S2. About 35 mg of the sample (35_PEI@Al_2O_3, PEI_196, or 40_Al_2O_3@PEI) was loaded in the sample holder of the DRIFTS chamber. The sample was activated at 100 °C for 3 h under 20 sccm N_2 after N_2 at the same flow rate flowed for 20 min at room temperature to flush out any physisorbed moisture, CO_2, and oxygen from ambient air. The temperature was then ramped down to 30 °C. For dry experiments, the inlet gas was switched to 400 ppm of CO_2/N_2, and spectra were collected with 16 scans at a resolution of 4 cm^{-1} every 1 min for the first 5 min and every 5 min for the rest of the adsorption period. This adsorption was carried out for 3 h, after which a desorption procedure identical to that of activation was employed. For humid experiments, the activation step was followed by pre-saturation at 30 °C during which the gas flow was switched from dry N_2 to humid N_2 with a relative humidity of 36.2 (±0.2)% RH. After 200 min of pre-saturation, adsorption was carried out under humid 400 ppm of CO_2/N_2, with spectra acquired. Water bubblers controlled the humidity of the feed gas during pre-saturation and adsorption steps at specific temperatures. Activated KBr in an adsorption gas stream (dry or humid 400 ppm of CO_2/N_2) was used as a background in these experiments.

Specific Heat Capacity. The specific heat capacity measurements were performed in a Netzsch (STA 449 F3 Jupiter) TGA/DSC following the ASTM E1269 "Standard test method for determining specific heat capacity by differential scanning calorimetry" protocol. About 25 mg of the sample was loaded into an open 85 μL alumina pan. The sample was activated under 50 mL[STP]/min of helium at 100 °C for 6 h and brought to room temperature. Under the same helium atmosphere, the temperature was ramped to 30 °C at the rate of 20 °C/min, held at 30 °C for 30 min, ramped to 100 °C at the rate of 10 °C/min and held at 100 °C for 30 min. The heat flux was recorded during this process. Before this experiment, the same experiment was performed with a pan containing a 4 mm sapphire disk with approximately the same thermal mass as the sample. All the experiments were corrected for buoyancy by performing the same experiment with an empty pan first. A sample heat flow profile of sapphire and PEI_196 is shown in Figure S3. The specific heat capacity of the sample, $C_P(s)$, is given by

$$C_P(s) = C_P(st)\frac{D_s \times W_{st}}{D_{st} \times W_s} \quad (1)$$

where D_s and D_{st} are the heat flow of the sample and sapphire standard, respectively, at a particular temperature, and W_s and W_{st} are the mass of the sample and sapphire standard, respectively. $C_P(st)$, the specific heat capacity of the sapphire standard at that temperature, was obtained from the literature.[54,55]

Heat of Adsorption. The heat of adsorption measurements were performed in a Netzsch (STA 449 F3 Jupiter) TGA/DSC. About 20 mg (±0.3 mg) of the sample was loaded into an open 85 μL alumina pan. The sample was purged with helium at room temperature for 20 min. Then, adsorbed moisture and CO_2 were removed by ramping the temperature to 100 °C at 10 °C/min under helium and holding for 3 h. Then, CO_2 adsorption was carried out at 25 °C under 90 mL[STP]/min of 400 ppm of CO_2/He mixture for 6 h. The same experiment was performed with an empty pan before the experiment to allow for buoyancy correction. The heat of adsorption of CO_2 in the presence of humidity could not be measured due to the instrument's limitations. Hence, it was estimated as described in Case 2 of Section S1.

RESULTS AND DISCUSSION

γ-Al_2O_3, Al_2O_3@PEI and PEI@Al_2O_3 Characterization. The self-supported PEI-based polymer sorbents were synthesized using ice-templating with and without alumina in the polymer matrix. The CO_2 capture mechanism, performance, and process energy requirements for deployment of the native PEI scaffold and Al_2O_3-loaded PEI scaffolds (denoted Al_2O_3@PEI) were compared to that of PEI supported on Al_2O_3 with different PEI loadings (denoted PEI@Al_2O_3). The loading of PEI in the impregnated sorbents was chosen to be within the range of PEI wt % in the neat, cross-linked PEI scaffold (35-40 wt %, the remaining portion is composed of PEGDGE). The impregnated sorbent comprises an Al_2O_3 matrix with PEI coated on it. The reduction in mass as a function of temperature and the corresponding loading of Al_2O_3 in the samples, as determined by the combustion TGA experiments, are presented in Figure S4. On the other hand, the Al_2O_3 loading as an additive in the PEI scaffolds was limited to 11.7 wt % to keep the Al_2O_3 content minimal and have Al_2O_3 only dispersed in a predominantly organic PEI−PEGDGE matrix.

The physical properties, such as specific surface area and pore volume of the Al_2O_3 and PEI@Al_2O_3 with different PEI loadings, along with the percent pore filling in the latter, are shown in Table 1. The specific surface area was estimated

Table 1. Physical Properties of Bare γ-Al_2O_3, PEI@Al_2O_3

Bare γ-Al_2O_3	
Particle size [μm]	9.59 ± 0.54[a]
Pore volume [cc/g]	0.64
Pore size (mode) [nm]	57.1
BET surface area [m^2/g]	96.8
35_PEI@Al_2O_3	
Pore filling [%]	81.9 (from N_2 physisorption)
	85.1 (from calculation)
40_PEI@Al_2O_3	
Pore filling [%]	92.6 (from N_2 physisorption)
	96.1 (from calculation)

[a]Mean particle size from SEM images.

using the BET equation.[56] The pore volume of Al_2O_3 and the percent pore filling of the PEI@Al_2O_3 samples were determined from the BJH analysis on the adsorption branch of nitrogen physisorption isotherm. The total pore volume is the total amount of nitrogen adsorbed at a P/P_0 of 0.998, also given by the cumulative pore volume from the BJH analysis. The nitrogen physisorption isotherms, BJH pore size distributions, and the cumulative pore volumes from BJH analysis are presented in Figure S5. A reduction in pore volume with the impregnation of Al_2O_3 with PEI was within the estimated range (Table 1) obtained based on the PEI loading and PEI density. This estimation was done assuming that all of PEI was impregnated within the pores of Al_2O_3. For the self-supported PEI scaffolds, due to the macroporous structure and the flexibility of the materials, the surface areas and the pore volumes could not be measured with the conventional cryogenic nitrogen physisorption method.

The morphology of the PEI scaffolds with and without Al_2O_3 additive was obtained from SEM and are shown in Figure 2. Ordered interconnected pore structures and lamellar stacking are observed in the lateral and cross-sectional images, respectively. The overall morphology of the sorbents with Al_2O_3 resembles the native PEI_196 scaffold synthesized in

https://doi.org/10.1021/cbe.3c00079
Chem Bio Eng. 2024, 1, 157−170

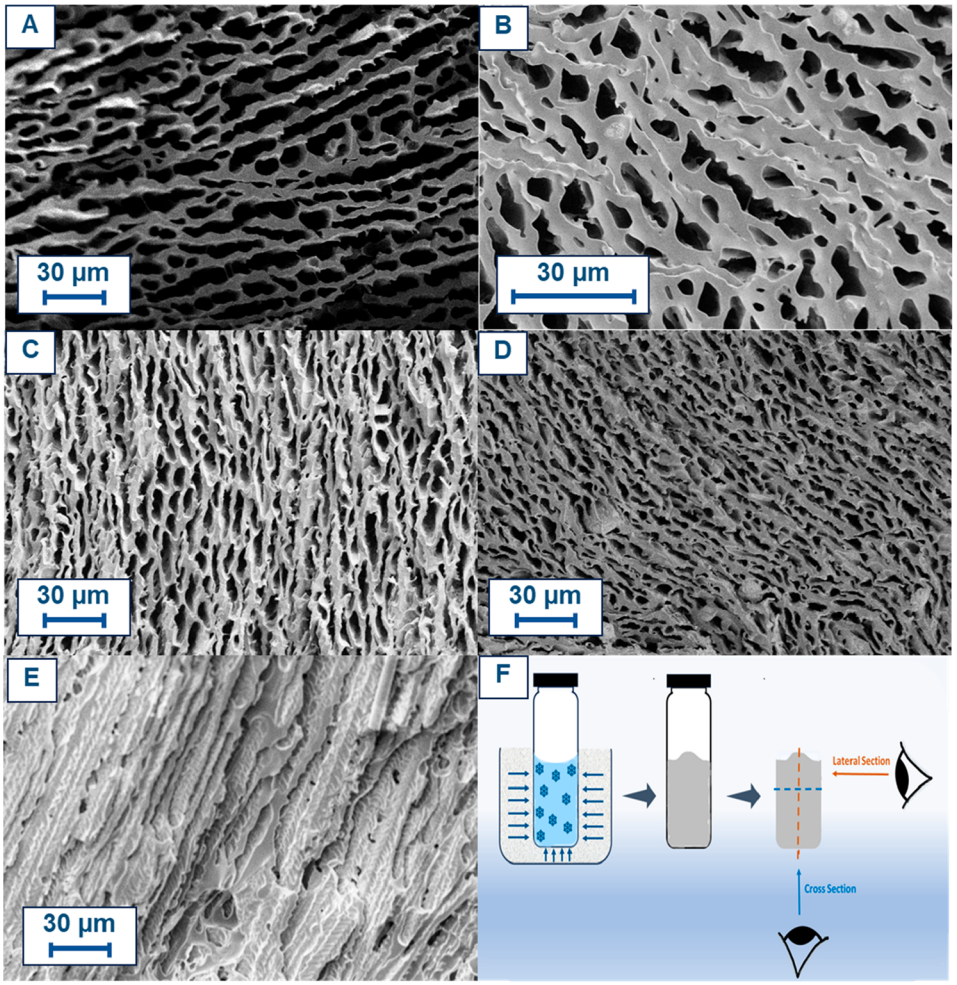

Figure 2. Morphology of self-supported PEI sorbents. (a) Lateral section of PEI_196. (b) Lateral section of 10_Al_2O_3@PEI. (c) Lateral section of 20_ Al_2O_3@PEI. (d) Lateral section of 40_ Al_2O_3@PEI. (e) Cross section of PEI_196. (f) Schematic of ice-templating showing temperature gradient and sectional views.

this and prior works.[48,49] However, the key differentiators among the sorbents are the size and distribution of pore lengths and pore wall thicknesses, which in turn determine the overall porosity of the sorbents. The PEI scaffolds' average pore length and pore wall thickness were estimated from SEM and are shown in Figures S6 and S7, respectively. The modal pore length and pore wall thickness of the PEI scaffolds are shown in Table 2. PEI_196 has the most extended pore length and a pore wall thickness of 5−10 and 4−6 μm, respectively. While 20_Al_2O_3@PEI and 40_Al_2O_3@PEI have the same modal pore length and pore wall thickness, both these parameters shift towards shorter lengths with the increase in the amount of Al_2O_3 in the PEI scaffolds, and the distributions of the pore length and pore wall thickness shift towards shorter dimensions, as seen in Figure S6 and Figure S7.

Table 2. Modal Pore Length and Pore Wall Thickness of PEI-Scaffolds, Estimated from SEM Images

Sample Name	Pore length [mode, μm]	Pore wall thickness [mode, μm]
PEI_196	5−10	4−6
10_ Al_2O_3@PEI	0−5	3−4
20_ Al_2O_3@PEI	0−5	2−3
40_ Al_2O_3@PEI	0−5	2−3

The average particle size of the commercial Sasol Al_2O_3 used is 9.6 μm, as seen from SEM (Figure S8). This size is comparable to and, in some cases, larger than the pore wall thickness of the PEI scaffolds. Hence, EDS was used to visualize the distribution of Al_2O_3 in the PEI scaffold. The EDS mapping of Al in 20_Al_2O_3@PEI is shown in Figure S9. Site A shows the presence of particulate Al_2O_3, and site B shows the presence of Al_2O_3, potentially in a digested form. The presence of Al_2O_3 in both these forms suggests that both the colligative effect resulting from the presence of Al_2O_3 as a "solute", and the effect of Al_2O_3 as a particle during the ice solidification process are potentially important in the ice-templating process.

While PEI_196 has the broadest distribution of pore wall thickness and pore length, the scaffolds with Al_2O_3 show a narrower distribution. Moreover, there is a leftward shift in pore wall thickness and pore size distribution with increased Al_2O_3 content in PEI scaffolds. This reduction in pore size and wall thickness can be attributed to a balancing act between two phenomena: (1) the effect of the colligative property, freezing point depression and (2) the hindrance to the cryo-concentration or ice-templating process. These two phenomena are further explained below.

https://doi.org/10.1021/cbe.3c00079
Chem Bio Eng. 2024, 1, 157−170

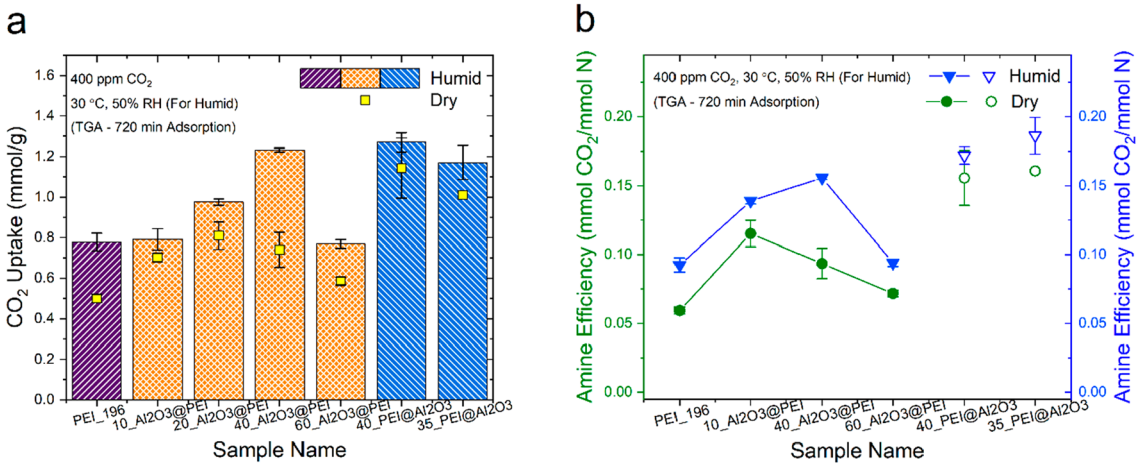

Figure 3. Performance of PEI scaffolds in comparison to PEI impregnated on Al_2O_3. (a) CO_2 uptake under dry (yellow squares) and humid conditions (50% RH, bars). (b) Amine efficiency for adsorption under dry and humid conditions. Filled symbols are for PEI scaffolds and hollow symbols are for PEI@Al_2O_3. All CO_2 adsorption was preceded by activation at 100 °C under the flow of N_2 for 30 min. The CO_2 concentration was 400 ppm, balanced by N_2. All gases were flowing at 90 mL[STP]/min. Purple, orange, and blue bars in (a) represent the PEI scaffold without Al_2O_3 additive, the PEI scaffold with Al_2O_3 additive, and PEI impregnated on Al_2O_3 i.e. PEI@Al_2O_3, respectively. The error bars are the standard deviations from three measurements of which two are from the same sample batch.

During the cryo-concentration process, the non-aqueous components, including the Al_2O_3 additive, are pushed to the non-frozen phase. The presence of solutes results in a depression in the freezing point of the non-frozen phase. This expulsion of solutes into the non-frozen phase continues until the depression in the freezing point is equal to the cross-linking temperature, and an equilibrium is achieved. Irrespective of the starting solute concentration, its concentration in the non-frozen phase remains the same, as determined by the above-mentioned equilibrium. However, the higher starting concentration of additives results in a larger size of the non-frozen phase, characterized by smaller pores and thicker pore walls. Hence, a reduction in the number of pores with smaller wall thicknesses and an increase in pores with shorter pore lengths is observed in all the sorbents with Al_2O_3. A similar phenomenon was observed by Kirsebom et al. while studying the presence of NaCl and $CaCl_2$ additives in the ice-templating of acrylamide.[59]

An increase in Al_2O_3 particle loading likely results in the less efficient movement of solutes into the nonfrozen phase owing to hindrance by the particle phase. We speculate that this results in a lesser number of pores with thicker walls. Additionally, the increase in Al_2O_3 particles also likely provides more nucleation sites, resulting in smaller pores. Thus, we speculate that the combination of the colligative property, freezing point depression, and hindrance to cryo-concentration in the increased presence of Al_2O_3 additive, results in a narrow distribution and left-ward shift towards lower pore sizes and pore wall thicknesses. It is to be noted that both these phenomena depend on the amount of solute (Al_2O_3 particle) loading in the ice-templating mixture.

CO_2 Adsorption Capacity. To understand the effect of the change in morphology of the PEI scaffolds in the presence of Al_2O_3 as an additive in the ice templating reaction, the CO_2 uptake of the PEI scaffolds under dry and humid conditions was measured using thermogravimetric analysis. The results are shown as squares in Figure 3a. The CO_2 uptake of PEI_196 under dry 400 ppm of CO_2/N_2 was found to be 0.5 mmol/gram of sorbent (referred to as mmol/g from here onwards) and increased with the Al_2O_3 loading up to a certain extent, beyond which the uptake began decreasing. The maximum CO_2 uptake among PEI scaffolds was 0.7 mmol/g for 20_Al_2O_3@PEI. This increase in CO_2 uptake with Al_2O_3 loading can be attributed to the PEI scaffolds' smaller pore size and pore wall thickness with the addition of Al_2O_3, as seen in Figures S6 and S7. A thinner pore wall can allow for better diffusion of CO_2 within the otherwise diffusion-limited cross-linked networks of the PEI scaffold. If the pore wall can be treated as a plane sheet of thickness l for a constant upstream and downstream concentration of the pore wall, the diffusion of CO_2 across the pore wall can be defined as

$$\frac{M_t}{M_\infty} = 1 - \frac{8}{\pi^2}\sum_{n=0}^{\infty}\frac{1}{(2n+1)^2}\exp\left\{-\frac{D(2n+1)^2\pi^2 t}{l^2}\right\} \quad (2)$$

where M_t is the total amount of CO_2 that enters the wall during time t, M_∞ is the corresponding amount during infinite time, and D is the diffusion coefficient.[60]

An earlier work by Ruthven and Loughlin showed that accurate diffusivities can be obtained for a wide distribution of diffusion lengths by superposition of the solution for each diffusion length within the distribution:[61]

$$\left.\frac{M_t}{M_\infty}\right|_{WTD} \approx \sum_i X_i \left.\frac{M_t}{M_\infty}\right|_{li} \quad (3)$$

where X_i is the weight fraction of pore walls with thickness l_i. The same superposition method applies to a broad range of pore sizes. Based on eqs 2 and 3, for the same mean or modal pore size, the CO_2 uptake would have a significant diffusion resistance contribution from the thicker pore walls and larger pores in a sample with broad pore size and wall thickness distribution, such as PEI_196, as compared to that of the sample with narrow distribution, as seen in 20_Al_2O_3@PEI.

This enhancement in diffusion is further manifested in the improvement in amine efficiency under dry conditions between PEI_196 and 20_Al_2O_3@PEI, shown in Figure 3b. A maximum amine efficiency of 0.12 mmol CO_2/mmol N was obtained for 20_Al_2O_3@PEI. Amine efficiency is the amount

https://doi.org/10.1021/cbe.3c00079
Chem Bio Eng. 2024, 1, 157−170

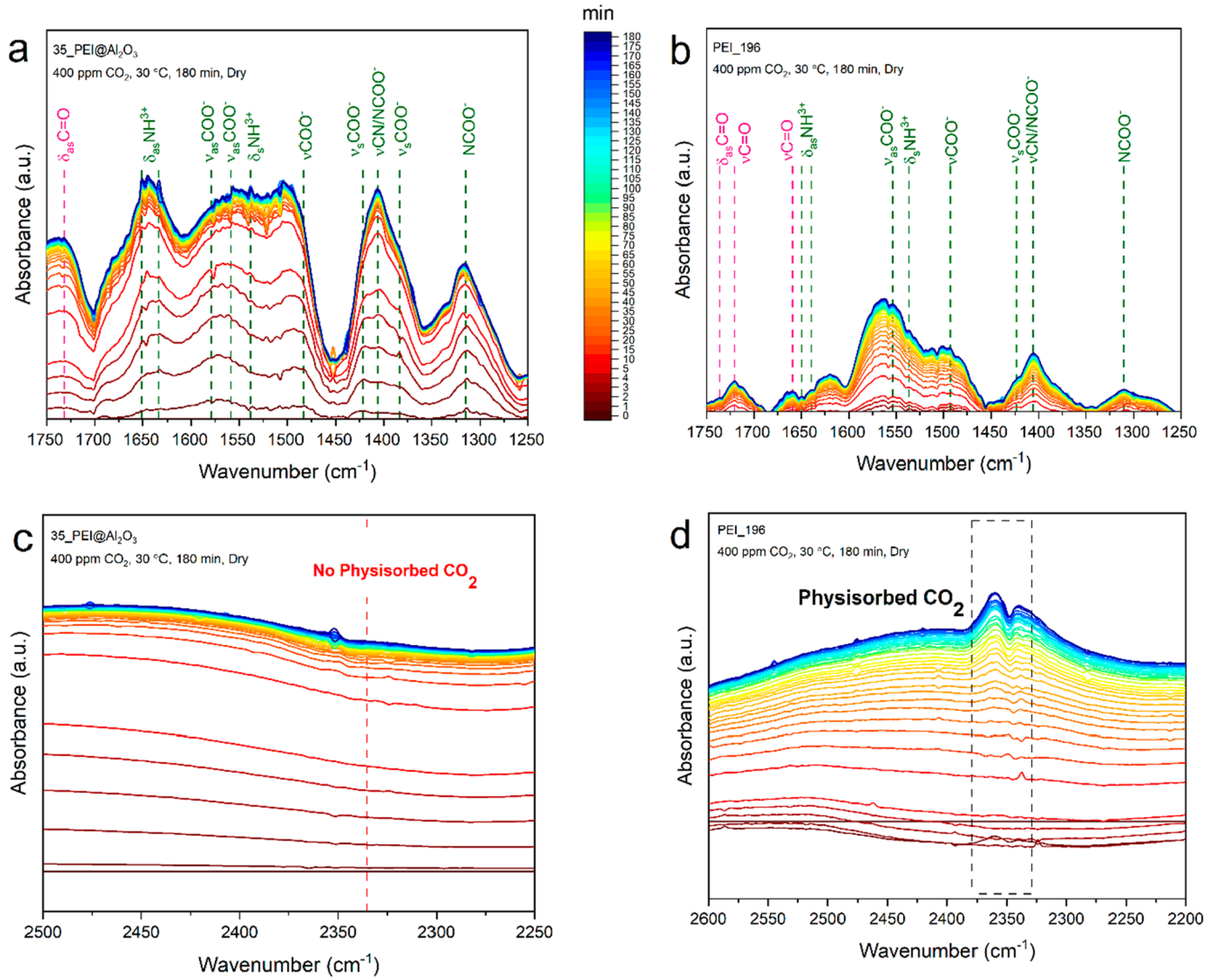

Figure 4. *In situ* FT-IR spectra of (a/c) 35_PEI@Al_2O_3 and (b/d) PEI_196 as a function of adsorption time at 30 °C with the activated sample as the background. The feed gas was dry 400 ppm of CO_2/N_2 at 20 sccm. Sample was activated at 100 °C under 20 sccm N_2 for 3 h. Pink represents carbamic acid (weekly bound) while green represents carbamate (strongly bound) and ammonium ions.

of CO_2 captured in mmol for every mmol of amine (primary, secondary, and tertiary), expressed as N atoms. A further increase in Al_2O_3 loading offers more ice nucleation sites in the templating process, potentially resulting in smaller but isolated pores. This is hypothesized to have resulted in a decrease in CO_2 uptake beyond 20_Al_2O_3@PEI and a corresponding decrease in amine efficiency. As a comparison, conventional PEI@Al_2O_3 sorbents have a higher CO_2 uptake and faster kinetics, as shown in Figure S10, because of the absence of cross-linked networks and the presence of more primary amines than the PEI scaffolds. While 40_PEI@Al_2O_3 has a higher uptake of 1.14 mmol/g of sorbent in comparison to 1.01 mmol/g of sorbent in the case of 35_PEI@Al_2O_3, the latter has a higher amine efficiency of 0.16 mmol CO_2/mmol N. The CO_2 uptake and amine efficiency of the impregnated amine sorbents are similar to those found in the literature.[51] The PEI@Al_2O_3 samples generally have at least 24.5% higher CO_2 uptake and 35% higher amine efficiency than the cross-linked PEI scaffolds under dry conditions. This reduced CO_2 sorption performance with an increase in amine loading in the PEI@Al_2O_3 series is likely due to the formation of PEI aggregates, resulting in more inaccessible amines in the sorbent with higher PEI loading.[62] A similar finding was observed by Moon et al. in PEI in functionalized SBA-15 supports.[62] The CO_2 uptake and amine efficiency of the impregnated amine sorbents are similar to those found in the literature.[51] The PEI@Al_2O_3 samples generally have at least 24% higher CO_2 uptake and 35% higher amine efficiency than the cross-linked PEI scaffolds under dry conditions.

Water Uptake. While ambient air contains ∼400 ppm of CO_2, it contains more water than CO_2, with absolute humidity varying from ∼0 g/m^3 (effectively never 0) to ∼84 g/m^3.[63] For the practical application of sorbents towards direct air capture, it is essential to understand the effect of humidity on the CO_2 capture performance of the sorbents. Humidity plays a vital role in amine-CO_2 adsorption mechanism and kinetics. Several studies have shown that humidity improves the CO_2 adsorption capacity of amine-based sorbents due to an increase in amine efficiency resulting from the formation of bicarbonate ions[64,65] and more carbamate ion pairs.[66−68] A study by Lee and co-workers showed that the increase in CO_2 uptake coming from the bicarbonate ions is minimal in some cases,[69]

https://doi.org/10.1021/cbe.3c00079
Chem Bio Eng. 2024, 1, 157−170

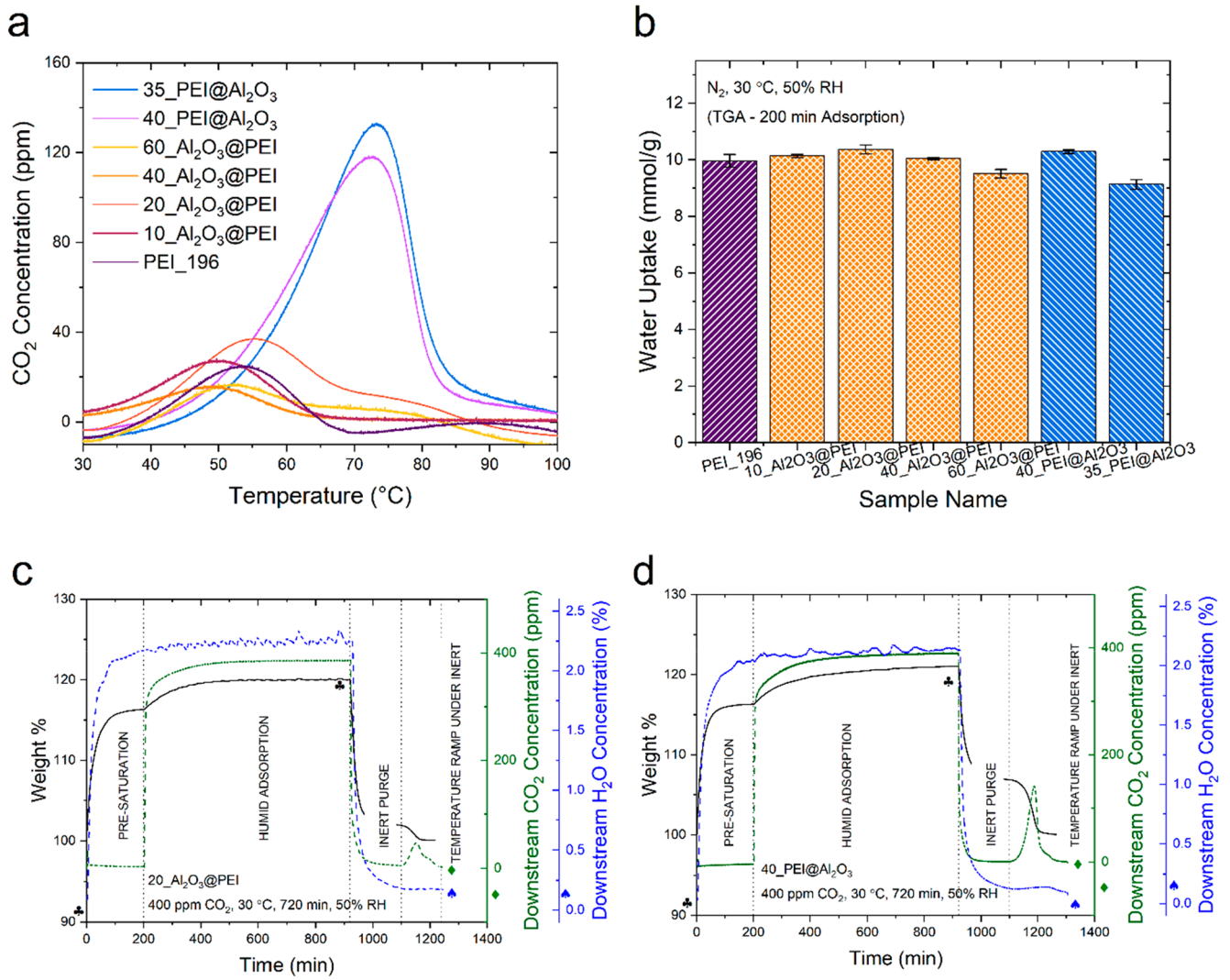

Figure 5. (a) Temperature-programmed desorption of CO_2 in PEI scaffolds and PEI@Al_2O_3 sorbents after pre-saturation with humid (50% RH) N_2 and adsorption of 400 ppm of CO_2/N_2 with 50% RH at 30 °C. (b) Water uptake under humid (50% RH) N_2. The error bars are the standard deviations from three measurements of which two are from the same sorbent batch. (c) TPD profile of 20_Al_2O_3@PEI along with pre-saturation and adsorption step showing change in weight% (black clubs), CO_2 (green diamonds), and water (blue spades) concentration. (d) TPD profile of 40_PEI@Al_2O_3 along with pre-saturation and adsorption step. Symbols same as in (c). All CO_2 and water adsorption was preceded by activation at 100 °C under a flow of N_2 for 30 min. All gases were flowing at 90 mL[STP]/min. Purple, orange, and blue bars in (b) represent the PEI scaffold without additive, PEI scaffold with Al_2O_3 additive, and PEI@Al_2O_3, respectively.

suggesting that the enhancement in the performance of the sorbent could be because of better arrangement and accessibility of amines in the presence of humidity. In addition, based on earlier work from our group, PEI scaffolds are known to undergo swelling in water, which could change the accessibility of amines.[48] Therefore, the effect of humidity on the CO_2 capture performance of the sorbents was probed. The bars in Figure 3a show the CO_2 uptake of PEI scaffolds and PEI@Al_2O_3 sorbents after 12 h of adsorption in 50% RH 400 ppm of CO_2/N_2. The uptake in PEI scaffolds shows a similar trend to that observed under dry conditions, however, with a right shift of the optimal Al_2O_3 loading. Among the scaffolds studied, 40_Al_2O_3@PEI had the highest CO_2 uptake of 1.23 mmol/g of sorbent. This CO_2 uptake is comparable to the highest CO_2 uptake achieved among the PEI@Al_2O_3 sorbents studied (1.27 mmol/g of sorbent, 40_PEI@ Al_2O_3). This increase in CO_2 uptake is attributed to improved amine utilization, as shown by an increased amine efficiency in the presence of humidity (Figure 3b). 40_Al_2O_3@PEI shows the highest amine efficiency among the sorbents, 0.16 mmol CO_2/mmol of N. Moreover, it is important to note that the amine efficiency of the PEI@Al_2O_3 sorbents is higher than that of the PEI scaffolds, suggesting that while the H_2O-induced loosening of cross-linked chains improves the CO_2 uptake and amine utilization, there are likely many tertiary amines in the sorbent that are not accessible to contribute to the CO_2 capture.

Mechanism of Amine–CO_2 Interaction. *In situ* DRIFTS experiments were used to probe the mechanism of amine-CO_2 interactions under dry and humid conditions, which can help understand the desorption behavior of the sorbents considered, as discussed in the next section. The spectra collected during dry and humid CO_2 adsorption on 35_PEI@Al_2O_3, PEI_196, and 20_Al_2O_3@PEI are shown in Figure 4. The spectra are produced by subtraction of the activated sample as the background to highlight the changes resulting from the adsorption of CO_2. Figure 4(a) shows the spectra for

https://doi.org/10.1021/cbe.3c00079
Chem Bio Eng. 2024, 1, 157−170

adsorption of dry 400 ppm of CO_2 on 35_PEI@Al_2O_3. The amine-CO_2 interaction is dominated by carbamate ions, while there seems to be some amount of carbamic acid produced as well. This is expected based on prior literature of amines supported on Al_2O_3.[50,70,71] The carbamic acid formation typically requires the involvement of a surface hydroxyl group or other H-bonding species for stabilization. The pore fill fraction of 35_PEI@Al_2O_3 is already above 80%, making it challenging to access many surface hydroxyl groups.

On the other hand, the carbamate ion formation requires two amines to react with one molecule of CO_2. With a high pore fill fraction, this mode of sorption becomes more probable. The carbamates have a more negative binding enthalpy (more thermodynamically favored), whereas the carbamic acids form weaker bonds with CO_2. Hence, 35_PEI@Al_2O_3 would require a relatively high temperature for regeneration. It is worth noting that the adsorption kinetics are fast, as evidenced by the clustering of spectra at the top of the figure from an early time of t = 15 min.

Figure 4b shows the adsorption spectra of 400 ppm dry CO_2 on PEI_196. The spectra are spread apart, suggesting slower CO_2 uptake kinetics than PEI@Al_2O_3. Like PEI@Al_2O_3, the IR spectra of PEI_196 show carbamate and carbamic acid bands. Among the two chemisorbed species, carbamate is more prevalent, although there are more carbamic acid bands found than in PEI@Al_2O_3. Owing to the hydroxyl groups on the polymer that can help stabilize the carbamic acid, the PEI scaffold has more carbamic acid bands than PEI@Al_2O_3. Meanwhile, the PEI_196 spectra have lower intensity than PEI@Al_2O_3, corroborating its lower CO_2 uptake under dry conditions. Furthermore, Figure 4c and d shows that a considerable fraction of CO_2 in the scaffold is physisorbed, and the ν_{as}(C═O) peak at 2335 cm^{-1} can be seen in PEI_196, while there was no evidence of the same peak in PEI@Al_2O_3 with amine aggregates. This physisorbed component could result from a smaller number of primary and secondary amines in the scaffold than in the native PEI resulting from the epoxide cross-linking reaction shown in Scheme 1. Figure S12a shows the *in situ* FT-IR spectra of 20_Al_2O_3@PEI. Similarly, Figure S12b–d shows the FT-IR spectra for humid CO_2 adsorption on 20_Al_2O_3@PEI, 35_PEI@Al_2O_3, and PEI_196, respectively. The humid adsorption spectra of 35_PEI@Al_2O_3 do not show a significant change compared to the dry adsorption spectra. The measured CO_2 uptake for this sample still shows a slight increase, potentially due to the lubrication by water, improving accessibility to amine sites. PEI_196 shows a significant increase in the spectral intensity of chemisorbed bands, resulting in an increase in CO_2 uptake in the presence of humidity. The carbamic acid contribution increases as well. Figure S12a and b compares dry and humid CO_2 uptakes in the PEI scaffold with Al_2O_3. The spectral intensities of the carbamate bands are similar under dry and humid conditions. However, the carbamic acid band at 1700 cm^{-1} is more pronounced in humid than in dry conditions. This is potentially due to better stabilization of carbamic acid groups by available hydroxyl groups under humid conditions. Moreover, it is important to note that the carbamic acid groups require less energy for desorption than carbamate ions.[50,72,73] This results in a lower energy of desorption in 20_Al_2O_3@PEI than PEI 196 (as discussed in the next section) and improved CO_2 uptake of 20_Al_2O_3@PEI under humid conditions. Moreover, carbamic acid formation requires only one amine to interact with every CO_2 molecule, unlike carbamate ion formation, which requires two amines to interact with every CO_2 molecule. Hence, the PEI scaffolds with the Al_2O_3 additive show an increase in amine efficiency in the presence of humidity.

Desorption Studies. While the adsorption capacity and amine efficiency are important parameters in evaluating a sorbent, the cost of operation is an essential factor in understanding the practicality of a sorbent technology. Most amine sorbents incorporate a temperature-swing adsorption process wherein heat is supplied to desorb the CO_2 at a higher temperature. This thermal regeneration can account for up to 50% of the total operating cost associated with the capture process.[17] Therefore, it is desirable for a sorbent to be regenerated at a lower temperature. Figure 5a shows the downstream concentration of CO_2 as measured by a gas analyzer after the sorbents saturated with humid (50% R.H.) 400 ppm of CO_2/N_2 were subjected to a slow temperature-programmed desorption at the rate of 0.5 °C/min in flowing N_2 (90 mL[STP]/min). The bed was pre-saturated with humid N_2 (50% R.H.) for 200 min at 30 °C before the adsorption step, and the water uptake of the sorbents was measured gravimetrically, as presented in Figure 5b. Based on the change in weight and the change in CO_2 and water concentration downstream using 20_Al_2O_3@PEI (Figure 5c) and 40_PEI@Al_2O_3 (Figure 5d), it was estimated that about 46% of the CO_2 was physisorbed and removed with a N_2 purge at room temperature in the case of 20_Al_2O_3@PEI, while all of the CO_2 in 40_PEI@Al_2O_3 was strongly bound and required a temperature ramp for desorption. The IR data discussed above also support this by the presence and absence of a broad physisorption peak in PEI_196 and PEI@Al_2O_3, respectively. In Figure 5a, the PEI@Al_2O_3 sorbents show a CO_2 desorption peak at 73 °C, while the PEI scaffolds show a desorption peak between 50 °C and 55 °C, further suggesting a weaker amine-CO_2 interaction and thereby lower energy of desorption in PEI scaffolds as compared to PEI@Al_2O_3. Higher water uptake in a particular sorbent during the pre-saturation and adsorption step could result in differing thermal energy transfer when adding heat to break the amine-CO_2 interactions. Therefore, it is best to compare the CO_2-amine binding energy of the sorbents based on the desorption temperature only if the water uptake is constant across the different sorbents. This was confirmed, as shown in Figure 5b. Additionally, the water concentration at the outlet of the TGA, as recorded by the LiCOR and presented in Figure 5c and d, shows no desorption of water during the adsorption of humid CO_2. Therefore, any weight change recorded during the adsorption of humid CO_2 is attributed to the CO_2 uptake by the sorbents.

Desorption Energy Requirement. The estimation of energy requirements in this work focuses only on the energy associated with the desorption process, i.e., the thermal energy, and does not account for other energy requirements in the form of pumping, fans, and blowers. This thermal analysis can help understand the economic feasibility of a temperature swing adsorption process with the sorbents studied. The total thermal energy during a temperature swing desorption process consists of sensible and latent heat. Sensible heat is the energy requirement associated with heating the sorbent and adsorbates (CO_2 for dry adsorption and CO_2 and water for humid adsorption) to the desired desorption temperature. The latent heat is the energy associated with the desorption of adsorbates from the adsorption sites. This can be approximated by the heat of adsorption of the adsorbates, assuming a

https://doi.org/10.1021/cbe.3c00079
Chem Bio Eng. 2024, 1, 157–170

negligible activation energy. While the specific heat capacity of adsorbates is available in the literature, their heat of adsorption on a specific sorbent and the specific heat capacity of that sorbent need to be estimated. The specific heat capacity of the PEI scaffolds and PEI@Al_2O_3 sorbents were estimated calorimetrically and are shown in Figure 6a as a function of temperature. Overall, the PEI scaffolds have a higher specific heat capacity than the PEI@Al_2O_3 sorbents, especially at lower temperatures below 90 °C, which is undesirable. Interestingly, unlike Al_2O_3 and PEI@Al_2O_3, the specific heat capacity of the PEI scaffolds does not increase with temperature and is comparable to or lower than that of PEI@Al_2O_3 beyond 90 °C.

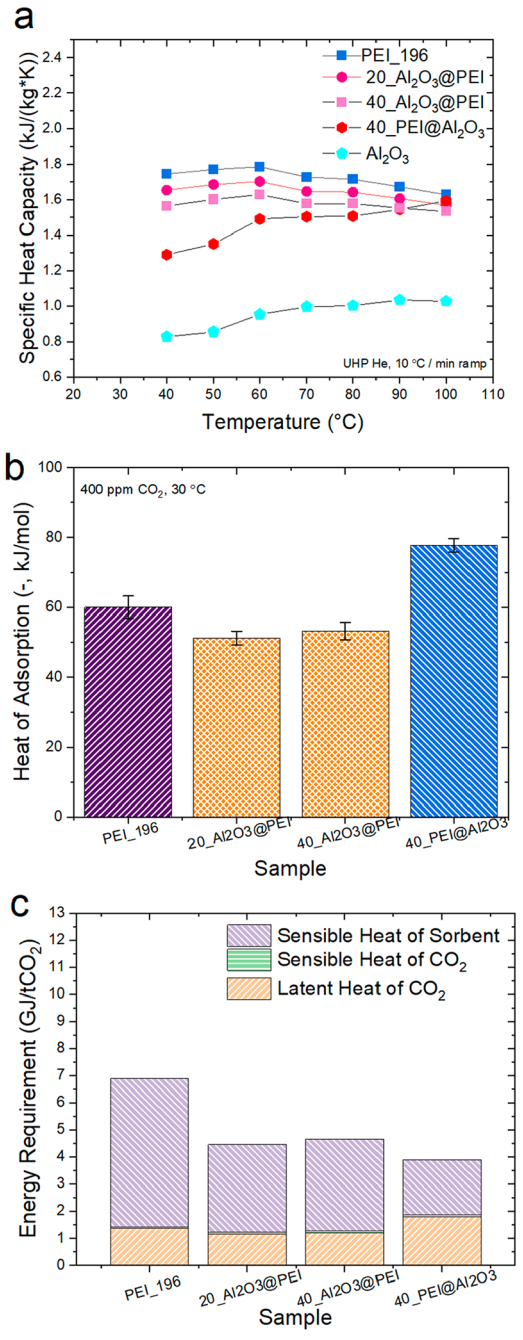

Figure 6. (a) Specific heat capacity of PEI scaffolds and 40_PEI@Al_2O_3 as a function of temperature after activation under N_2 at 100 °C for 6 h. (b) Heat of 400 ppm of CO_2 adsorption for PEI scaffolds and 40_PEI@Al_2O_3. (c) Thermal energy requirements for desorption of dry CO_2 including sensible heat components (of sorbent in purple, CO_2 in green) and latent heat of CO_2 (orange). The error bars in (b) are the standard deviations from three measurements of which two are from the same sorbent batch.

To estimate the latent heat of sorption, two cases were considered: (1) adsorption of CO_2 in dry conditions and (2) adsorption of CO_2 and water in humid conditions. For case 1, the heat of adsorption of CO_2 was measured calorimetrically and shown in Figure 6b. The PEI scaffolds show a heat of adsorption ranging between −50 and −60 kJ/mol while 40_PEI@Al_2O_3 has a heat of adsorption of −78 kJ/mol. The lower heat of adsorption of the PEI scaffolds compared to that of PEI@Al_2O_3 sorbent suggests a weaker amine-CO_2 interaction and a lower energy penalty for desorption of CO_2 in the former. This corroborates the lower temperature requirement for the desorption of CO_2 in PEI scaffolds, as seen in the temperature-programmed desorption in Figure 5a. Among the PEI scaffolds, the ones with Al_2O_3 additive show a comparable heat of adsorption (~52 kJ/mol), modestly lower than that of the PEI scaffold without the alumina additive (60 kJ/mol).

The thermal energy penalty associated with the desorption process was determined using the above specific heat capacity, the heat of adsorption, and the adsorption capacity shown in the earlier section. The results are shown in Figure 6c. Further details and model calculations are shown in Supporting Information (SI) Section S1. PEI_196 has the highest energy penalty among the sorbents studied, with a total of 6.9 GJ/t_{CO2}, while 40_PEI@Al_2O_3 has the lowest energy penalty of 3.9 GJ/t_{CO2}. The primary energy contributor in PEI scaffolds is the sensible heat of the sorbent, constituting 72−79% of the overall heat duty. With every additional cycle required to achieve a tonne of CO_2 capture, the sorbent would have to be heated and an additional sensible heat penalty would have to be paid. While rapid temperature swing cycles can increase the productivity in tonnes of CO_2 captured per hour, it may not be the most effective strategy for PEI scaffolds from a cost perspective unless it is coupled with strategies to improve the sorbent adsorption capacity and kinetics. It is desirable to reduce the ratio of sensible heat (GJ) and productivity (tonne of CO_2/day). The improvement in adsorption capacity and kinetics could be achieved by retaining more primary and secondary amines in the PEI scaffold during the cross-linking reaction shown in Scheme 1. However, the presence of more primary amines in the sorbent would result in stronger amine-CO_2 binding energy, higher energy of desorption, and, thereby, higher latent heat of CO_2, which is the second highest contributor to the energy penalty. Secondary amines could offer a "sweet spot" between the sensible heat of the sorbent and the latent heat of CO_2. The sensible heat of CO_2, directly proportional to the amount of CO_2 adsorbed, has the least contribution in all the sorbents studied. Therefore, an increase in adsorption capacity would have a negligible negative impact on the energy penalty. Bare Al_2O_3 has a low C_P of about 1 J K^{-1} mol^{-1}. That, combined with an improved CO_2 uptake in the presence of Al_2O_3, results in a dramatic reduction in sensible heat of the sorbent, making the PEI scaffolds with Al_2O_3 a close second after the PEI impregnated sorbent in energy efficiency. It is noted that while the PEI scaffolds are already in the form of a structured contactor, the latter would require binders to shape them, which will reduce their overall energy efficiency.

https://doi.org/10.1021/cbe.3c00079
Chem Bio Eng. 2024, 1, 157−170

Case 2 involves adsorption of humid (50% R.H.) 400 ppm of CO_2. Hence, the water uptake of the sorbents was measured for a wide range of partial pressures. The isotherms are presented in Figure 7a. The inset shows similar water uptake for the sorbents at lower partial pressures, in line with the findings from thermogravimetric estimation of water uptake. PEI scaffolds showed higher water uptake at higher humidity above 50% R.H., possibly due to swelling of the polymer network, which is not the case with PEI@Al_2O_3 sorbents. Adsorption of CO_2 under humid conditions consists of sensible and latent heat components from CO_2 and H_2O, as well as the sensible heat of the sorbent. The estimation of sensible heat followed a procedure similar to case 1. A representative case with PEI_196 is shown in SI Section S1.

Moreover, the heat of water adsorption for the PEI scaffolds and 40_PEI@Al_2O_3 was determined from water uptakes at three different temperatures (30 °C, 40 °C, and 50 °C), as shown in Figure 7b. The water uptake isotherms at individual temperatures are shown in Figure S11, with details on the heat of adsorption shown in SI Section S2. The PEI scaffolds' water uptake is ~10 mmol/g (as shown in Figure 5b) at 50% RH. The heat of water adsorption corresponding to this water loading in Figure 5a was −44 to −45 kJ/mol. This is comparable to the latent heat of bulk water, which is −43.8 kJ/mol, suggesting that most interactions are between water molecules rather than between water and active amine sites.

Interestingly, the heat of adsorption of the PEI scaffolds increases until a water loading of 10 mmol/g, potentially from the loosening and re-arrangement of the otherwise highly tangled cross-linked networks. This phenomenon would expose more hydrophilic amine sites at lower surface coverage that would otherwise be inaccessible to the water molecules. With further water loading, the heat of adsorption in PEI_196 tends to plateau around the heat of vaporization of bulk water.

The energy of desorption of humid CO_2 was approximated using the method explained in SI Section S1 Case 2. Finally, incorporating the sensible heat of the sorbent, CO_2, H_2O, and latent heat of CO_2 and H_2O, the total thermal energy required for desorption of humid CO_2 at 50% RH was estimated and shown in Table S7. PEI_196 has the highest energy penalty of 20.6 GJ/tCO_2, while 40_Al_2O_3@PEI has the lowest energy penalty of 13.19 GJ/t_{CO2}. The sorbent with PEI impregnated on Al_2O_3, 40_PEI@Al_2O_3, has the second lowest energy penalty at 13.43 GJ/t_{CO2}. The latent heat of water is the main contributor among the five energy components, consisting of about 66% to 69% of the total energy requirement. This energy requirement assumes that all the adsorbed water is removed along with the CO_2, which is undesirable. In practical application, the energy penalty associated with the latent heat of water can be minimized by deploying steam stripping. Figure 7c and Table S8 show the reduced energy penalty. As in the case of adsorption in dry conditions, the top two contributions to the total energy requirement for desorption are from the sensible heat of the sorbent and the latent heat of CO_2, while the sensible heat of CO_2 has the least contribution (a key driver for the use of "all sorbent" contactors such as these). PEI_196 has the highest energy penalty of the sample studied, 6.83 GJ/t_{CO2}. While the sensible heat remained the major contributor in sorbents with no or minimal Al_2O_3, the bottleneck in 40_PEI@Al_2O_3 is the latent heat of CO_2, since the amines and CO_2 can form stronger carbamate ions in the presence of humidity, as compared to the weaker carbamic acid. This bottleneck is minimized in PEI scaffolds with Al_2O_3

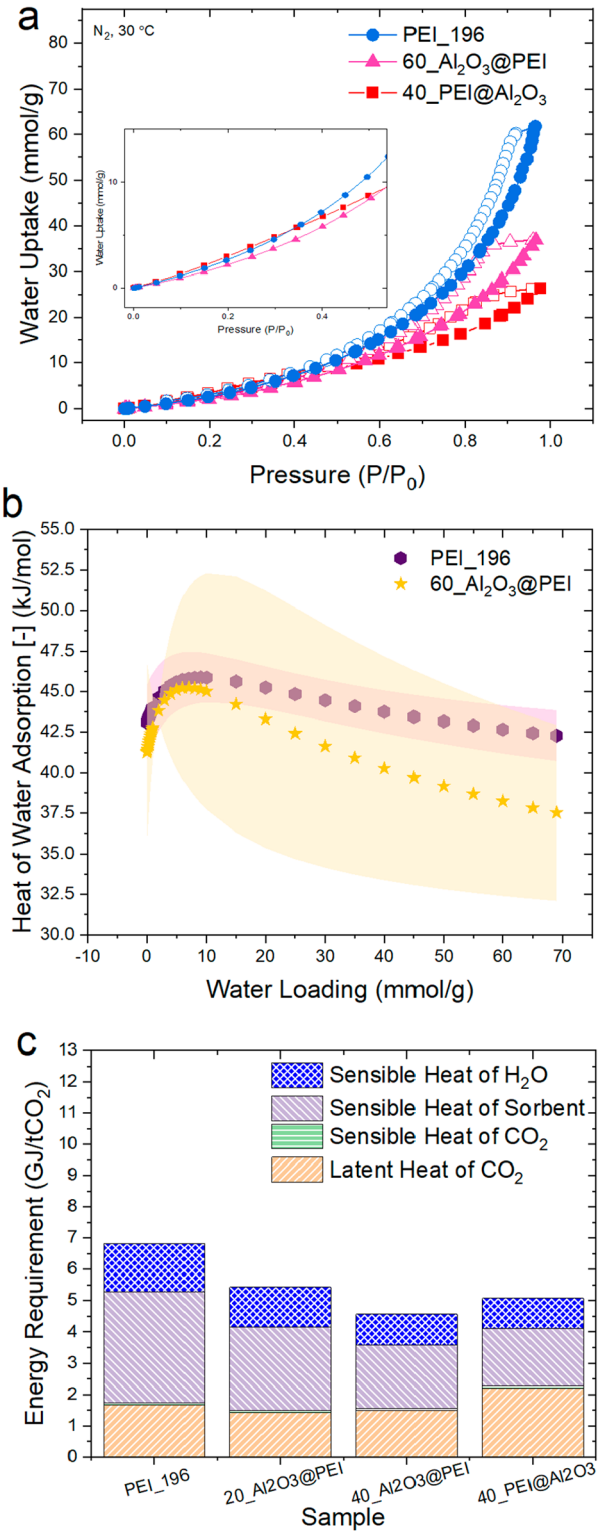

Figure 7. Effect of humidity: (a) Water uptake isotherm of PEI impregnated sorbent, PEI scaffold with and without Al_2O_3. (b) Heat of water adsorption of PEI scaffolds with and without Al_2O_3, with the bands showing error margins from three measurements on the same sample. (c) Thermal energy requirement for desorption of humid CO_2 after adsorption from 50% RH 400 ppm of CO_2/N_2. Contributions include sensible heat components (of water in blue, sorbent in purple, CO_2 in green) and latent heat of CO_2 (orange). By assuming desorption is using steam, latent heat of H_2O is excluded.

https://doi.org/10.1021/cbe.3c00079
Chem Bio Eng. 2024, 1, 157−170

as an additive since physisorption and formation of weekly bound carbamic acid species are promoted instead of strongly bound carbamate ions. As a result, 40_PEI@Al_2O_3 has a higher energy penalty (5.08 GJ/t_{CO2}) than 40_Al_2O_3@PEI (4.57 GJ/t_{CO2}), the least among the sorbents studied. This is despite 40_PEI@Al_2O_3 having a higher CO_2 uptake than the latter. Finally, it is worth noting that all the water uptake and energy calculations assume pseudo-equilibrium sorption. With a shorter sorption time and smaller working capacity, while there is potential to reduce the energy penalty associated with water sorption, it is also essential to have a good CO_2 working capacity for reasonable productivity.

SUMMARY AND CONCLUSIONS

Self-supported PEI scaffolds with and without Al_2O_3 as an additive were synthesized in this work, and their performance was evaluated for direct air capture of CO_2. Al_2O_3 as an additive affected the morphology of the ice-templated sorbent. This can effectively improve sorbent performance for CO_2 capture, especially in ultra-dilute conditions. It was shown that a small amount of Al_2O_3 can significantly increase the CO_2 uptake, even when interspersed in a polymer matrix. The main effect of the additive was a reduction in pore length and pore wall thickness, narrowing their distribution. This change in morphology helps improve the sample's CO_2 uptake. Although the CO_2 uptake of the PEI scaffolds is lower than that of conventional PEI-impregnated on alumina under dry conditions, the CO_2 uptake of the best-performing Al_2O_3-incorporated scaffold is comparable to that of the benchmark material under humid conditions. PEI scaffolds with the alumina additive also have a lower thermal energy requirements than the impregnated amine sorbent, at approximately 4.57 GJ/t_{CO2}, making them promising candidates for direct air capture applications. However, this energy requirement assumes that the desorption is carried out using steam.

A limitation of this work is that the results here only show that the PEI scaffolds are useful for CO_2 capture from a feed with a specific range of relative humidity, around 50% RH. While they do not perform better than the PEI-impregnated sorbents under dry conditions, they would adsorb larger amounts of water than the conventional sorbents at higher humidity levels, thereby potentially increasing the energy requirement for sorbent regeneration. Furthermore, two additional things should be noted: (i) All the performance and energy comparisons for the PEI scaffolds were made against powdered PEI@Al_2O_3 sorbents. The performance of the benchmark powders may be compromised by adding binders, which is likely necessary to incorporate them into structured contactors. (ii) Water uptake measurements were all for pseudo-equilibrium conditions, while in practical applications, cycle time would be shorter and can, therefore, limit the water uptake to a certain extent. Finally, steam stripping has been proposed as a general method of regeneration. However, the desorption studies conducted here were done under an inert gas environment. Therefore, a demonstration of steam stripping and utilizing the latent heat of condensing water is necessary as part of future work.

ASSOCIATED CONTENT

Supporting Information

The Supporting Information is available free of charge at https://pubs.acs.org/doi/10.1021/cbe.3c00079.

^{13}C NMR spectrum of 60 kDa b-PEI, experimental setup for CO_2 uptake measurements and DRIFTS, sample heat profile in TGA-DSC, TGA curves, nitrogen physisorption isotherm, pore size distribution of Al_2O_3 and PEI scaffolds, pore wall thickness distribution of PEI scaffolds, SEM images and EDS of Al_2O_3 and Al_2O_3-incorporated PEI scaffolds, CO_2 and water uptake curves, *in situ* FT-IR spectra of sorbents under humid conditions, estimation of thermal energy requirement (PDF)

AUTHOR INFORMATION

Corresponding Authors

Christopher W. Jones − *School of Chemical & Biomolecular Engineering, Georgia Institute of Technology, Atlanta, Georgia 30332, United States;* orcid.org/0000-0003-3255-5791; Email: cjones@chbe.gatech.edu

Ryan P. Lively − *School of Chemical & Biomolecular Engineering, Georgia Institute of Technology, Atlanta, Georgia 30332, United States;* orcid.org/0000-0002-8039-4008; Email: ryan.lively@chbe.gatech.edu

Authors

Pavithra Narayanan − *School of Chemical & Biomolecular Engineering, Georgia Institute of Technology, Atlanta, Georgia 30332, United States;* orcid.org/0000-0002-9045-2830

Pranav Guntupalli − *School of Chemical & Biomolecular Engineering, Georgia Institute of Technology, Atlanta, Georgia 30332, United States*

Complete contact information is available at: https://pubs.acs.org/10.1021/cbe.3c00079

Notes

The authors declare the following competing financial interest(s): C.W.J. has a financial interest in several companies that seek to commercialize CO_2 capture from air. This work is not affiliated with any such firms. C.W.J. has a conflict-of-interest management plan in place at Georgia Tech.

ACKNOWLEDGMENTS

The authors thank Yoseph Guta, Georgia Institute of Technology, for useful discussions. This work was supported by the Center for Understanding and Controlling Accelerated and Gradual Evolution of Materials for Energy (UNCAGE-ME), an Energy Frontier Research Center funded by the U.S. Department of Energy, Office of Science, Office of Basic Energy Sciences, under Award No. DE-SC0012577. This work was performed in part at the Georgia Tech Institute for Electronics and Nanotechnology, a member of the National Nanotechnology Coordinated Infrastructure (NNCI), which is supported by the National Science Foundation (ECCS-2025462).

REFERENCES

(1) Lackner, K.; Ziock, H.-J.; Grimes, P. *Carbon Dioxide Extraction from Air: Is It An Option?* United States, 1999.

(2) Yu, C. H.; Huang, C. H.; Tan, C. S. A Review of CO_2 Capture by Absorption and Adsorption. *Aerosol Air Qual Res.* **2012**, *12* (5), 745−769.

(3) Gelles, T.; Lawson, S.; Rownaghi, A. A.; Rezaei, F. Recent Advances in Development of Amine Functionalized Adsorbents for CO_2 Capture. *Adsorption* **2020**, *26* (1), 5−50.

(4) Darunte, L. A.; Terada, Y.; Murdock, C. R.; Walton, K. S.; Sholl, D. S.; Jones, C. W. Monolith-Supported Amine-Functionalized Mg_2(Dobpdc) Adsorbents for CO_2 Capture. *ACS Appl. Mater. Interfaces* **2017**, *9* (20), 17042−17050.
(5) Sakwa-Novak, M. A.; Yoo, C. J.; Tan, S.; Rashidi, F.; Jones, C. W. Poly(Ethylenimine)-Functionalized Monolithic Alumina Honeycomb Adsorbents for CO_2 Capture from Air. *ChemSusChem* **2016**, *9* (14), 1859−1868.
(6) Chen, Z.; Deng, S.; Wei, H.; Wang, B.; Huang, J.; Yu, G. Polyethylenimine-Impregnated Resin for High CO_2 Adsorption: An Efficient Adsorbent for CO_2 Capture from Simulated Flue Gas and Ambient Air. *ACS Appl. Mater. Interfaces* **2013**, *5* (15), 6937−6945.
(7) Sujan, A.; Kumar, D. R.; Sakwa-Novak, M. A.; Ping, E. W.; Hu, B.; Park, S. J.; Jones, C. W. Poly(Glycidyl Amine) Loaded SBA-15 Sorbents for CO_2 Capture from Dilute and Ultra-Dilute Gas Mixtures. *ACS Appl. Polym. Mater.* **2019**, *1*, 3137.
(8) Lee, W. H.; Zhang, X.; Banerjee, S.; Jones, C. W.; Realff, M. J.; Lively, R. P. Sorbent-Coated Carbon Fibers for Direct Air Capture Using Electrically Driven Temperature Swing Adsorption. *Joule* **2023**, *7* (6), 1241−1259.
(9) Fisher, J. C.; Tanthana, J.; Chuang, S. S.C. Oxide-Supported Tetraethylenepentamine for CO2 Capture. *Environ. Prog. Sustain Energy* **2009**, *28* (4), 589−598.
(10) Gebald, C.; Wurzbacher, J. A.; Tingaut, P.; Zimmermann, T.; Steinfeld, A. Amine-Based Nanofibrillated Cellulose as Adsorbent for CO_2 Capture from Air. *Environ. Sci. Technol.* **2011**, *45* (20), 9101−9108.
(11) Sanz-Pérez, E. S.; Murdock, C. R.; Didas, S. A.; Jones, C. W. Direct Capture of CO_2 from Ambient Air. *Chem. Rev.* **2016**, *116* (19), 11840−11876.
(12) Shi, X.; Xiao, H.; Azarabadi, H.; Song, J.; Wu, X.; Chen, X.; Lackner, K. S. Sorbents for the Direct Capture of CO_2 from Ambient Air. *Angew. Chem., Int. Ed.* **2020**, *59* (18), 6984−7006.
(13) Wilson, S. M. W.; Tezel, F. H. Direct Dry Air Capture of CO_2 Using VTSA with Faujasite Zeolites. *Ind. Eng. Chem. Res.* **2020**, *59* (18), 8783−8794.
(14) McQueen, N.; Gomes, K. V.; McCormick, C.; Blumanthal, K.; Pisciotta, M.; Wilcox, J. A Review of Direct Air Capture (DAC): Scaling up Commercial Technologies and Innovating for the Future. *Progress in Energy* **2021**, *3* (3), No. 032001.
(15) Elfving, J.; Bajamundi, C.; Kauppinen, J.; Sainio, T. Modelling of Equilibrium Working Capacity of PSA, TSA and TVSA Processes for CO_2 Adsorption under Direct Air Capture Conditions. *Journal of CO2 Utilization* **2017**, *22* (October), 270−277.
(16) Veselovskaya, J. V.; Parunin, P. D.; Netskina, O. V.; Okunev, A. G. A Novel Process for Renewable Methane Production: Combining Direct Air Capture by K_2CO_3/Alumina Sorbent with CO_2 Methanation over Ru/Alumina Catalyst. *Top Catal* **2018**, *61* (15−17), 1528−1536.
(17) Chowdhury, S.; Kumar, Y.; Shrivastava, S.; Patel, S. K.; Sangwai, J. S. A Review on the Recent Scientific and Commercial Progress on the Direct Air Capture Technology to Manage Atmospheric CO_2 Concentrations and Future Perspectives. *Energy Fuels* **2023**, *37*, 10733−10757.
(18) Kulkarni, A. R.; Sholl, D. S. Analysis of Equilibrium-Based TSA Processes for Direct Capture of CO_2 from Air. *Ind. Eng. Chem. Res.* **2012**, *51* (25), 8631−8645.
(19) Didas, S. A.; Zhu, R.; Brunelli, N. A.; Sholl, D. S.; Jones, C. W. Thermal, Oxidative and CO_2 Induced Degradation of Primary Amines Used for CO_2 Capture: Effect of Alkyl Linker on Stability. *J. Phys. Chem. C* **2014**, *118* (23), 12302−12311.
(20) Sandhu, N. K.; Pudasainee, D.; Sarkar, P.; Gupta, R. Steam Regeneration of Polyethylenimine-Impregnated Silica Sorbent for Postcombustion CO_2 Capture: A Multicyclic Study. *Ind. Eng. Chem. Res.* **2016**, *55* (7), 2210−2220.
(21) Direct Air Capture - Energy System. *IEA*. https://www.iea.org/energy-system/carbon-capture-utilisation-and-storage/direct-air-capture#tracking (accessed 2023-09-24).
(22) International Energy Agency. *CO_2 Emissions in 2022*. www.iea.org (accessed 2023-09-26).
(23) Erans, M.; Sanz-Pérez, E. S.; Hanak, D. P.; Clulow, Z.; Reiner, D. M.; Mutch, G. A. Direct Air Capture: Process Technology, Techno-Economic and Socio-Political Challenges. *Energy Environ. Sci.* **2022**, *15* (4), 1360−1405.
(24) Leonzio, G.; Fennell, P. S.; Shah, N. A Comparative Study of Different Sorbents in the Context of Direct Air Capture (DAC): Evaluation of Key Performance Indicators and Comparisons. *Applied Sciences (Switzerland)* **2022**, *12* (5), 2618−2642.
(25) Zhao, Y.; Zhou, J.; Fan, L.; Chen, L.; Li, L.; Xu, Z. P.; Qian, G. Indoor CO_2 Control through Mesoporous Amine-Functionalized Silica Monoliths. *Ind. Eng. Chem. Res.* **2019**, *58* (42), 19465−19474.
(26) Thakkar, H.; Eastman, S.; Hajari, A.; Rownaghi, A. A.; Knox, J. C.; Rezaei, F. 3D-Printed Zeolite Monoliths for CO_2 Removal from Enclosed Environments. *ACS Appl. Mater. Interfaces* **2016**, *8* (41), 27753−27761.
(27) Guo, X.; Ding, L.; Kanamori, K.; Nakanishi, K.; Yang, H. Functionalization of Hierarchically Porous Silica Monoliths with Polyethyleneimine (PEI) for CO_2 Adsorption. *Microporous and Mesoporous Materials* **2017**, *245*, 51−57.
(28) Thakkar, H.; Eastman, S.; Al-Naddaf, Q.; Rownaghi, A. A.; Rezaei, F. 3D-Printed Metal-Organic Framework Monoliths for Gas Adsorption Processes. *ACS Appl. Mater. Interfaces* **2017**, *9* (41), 35908−35916.
(29) Lawson, S.; Griffin, C.; Rapp, K.; Rownaghi, A. A.; Rezaei, F. Amine-Functionalized MIL-101 Monoliths for CO_2 Removal from Enclosed Environments. *Energy Fuels* **2019**, *33* (3), 2399−2407.
(30) Fan, Y.; Rezaei, F.; Labreche, Y.; Lively, R. P.; Koros, W. J.; Jones, C. W. Stability of Amine-Based Hollow Fiber CO_2 Adsorbents in the Presence of NO and SO_2. *Fuel* **2015**, *160*, 153−164.
(31) Mansourizadeh, A.; Ismail, A. F.; Abdullah, M. S.; Ng, B. C. Preparation of Polyvinylidene Fluoride Hollow Fiber Membranes for CO_2 Absorption Using Phase-Inversion Promoter Additives. *J. Memb Sci.* **2010**, *355* (1−2), 200−207.
(32) He, H.; Hou, X.; Ma, B.; Zhuang, L.; Li, C.; He, S.; Chen, S. The Oxidation of Viscose Fiber Optimized by Response Surface Methodology and Its Further Amination with PEI for CO_2 Adsorption. *Cellulose* **2016**, *23* (4), 2539−2548.
(33) Keller, L.; Lohaus, T.; Abduly, L.; Hadler, G.; Wessling, M. Electrical Swing Adsorption on Functionalized Hollow Fibers. *Chemical Engineering Journal* **2019**, *371* (April), 107−117.
(34) Lively, R. P.; Chance, R. R.; Kelley, B. T.; Deckman, H. W.; Drese, J. H.; Jones, C. W.; Koros, W. J. Hollow Fiber Adsorbents for CO_2 Removal from Flue Gas. *Ind. Eng. Chem. Res.* **2009**, *48* (15), 7314−7324.
(35) Sujan, A. R.; Pang, S. H.; Zhu, G.; Jones, C. W.; Lively, R. P. Direct CO_2 Capture from Air Using Poly(Ethylenimine)-Loaded Polymer/Silica Fiber Sorbents. *ACS Sustain Chem. Eng.* **2019**, *7* (5), 5264−5273.
(36) Min, Y. J.; Ganesan, A.; Realff, M. J.; Jones, C. W. Direct Air Capture of CO_2 Using Poly(Ethyleneimine)-Functionalized Expanded Poly(Tetrafluoroethylene)/Silica Composite Structured Sorbents. *ACS Appl. Mater. Interfaces* **2022**, *14* (36), 40992−41002.
(37) Akhtar, F.; Ogunwumi, S.; Bergström, L. Thin Zeolite Laminates for Rapid and Energy-Efficient Carbon Capture. *Sci. Rep* **2017**, *7* (1), 10988.
(38) Rezaei, F.; Webley, P. Optimum Structured Adsorbents for Gas Separation Processes. *Chem. Eng. Sci.* **2009**, *64* (24), 5182−5191.
(39) Vainerman, E. S.; Lozinsky, V. I.; Rogozhin, S. V. Study of Cryostructurization of Polymer Systems. *Colloid Polym. Sci.* **1981**, *259* (12), 1198−1201.
(40) Okay, O.; Lozinsky, V. I. Synthesis and Structure−Property Relationships of Cryogels. *Advances in Polymer Science* **2014**, *263*, 103−157.
(41) Chatterjee, S.; Potdar, A.; Kuhn, S.; Kumaraswamy, G. Preparation of Macroporous Scaffolds with Holes in Pore Walls and Pressure Driven Flows through Them. *RSC Adv.* **2018**, *8* (44), 24731−24739.

https://doi.org/10.1021/cbe.3c00079
Chem Bio Eng. 2024, 1, 157−170

(42) Zhang, H.; Hussain, I.; Brust, M.; Butler, M. F.; Rannard, S. P.; Cooper, A. I. Aligned Two- and Three-Dimensional Structures by Directional Freezing of Polymers and Nanoparticles. *Nat. Mater.* **2005**, *4* (10), 787−793.
(43) Gao, H. L.; Xu, L.; Long, F.; Pan, Z.; Du, Y. X.; Lu, Y.; Ge, J.; Yu, S. H. Macroscopic Free-Standing Hierarchical 3D Architectures Assembled from Silver Nanowires by Ice Templating. *Angewandte Chemie - International Edition* **2014**, *53* (18), 4561−4566.
(44) Han, J.; Yang, J.; Gao, W.; Bai, H. Ice-Templated, Large-Area Silver Nanowire Pattern for Flexible Transparent Electrode. *Adv. Funct Mater.* **2021**, *31* (16), 2010155.
(45) Munch, E.; Saiz, E.; Tomsia, A. P.; Deville, S. Architectural Control of Freeze-Cast Ceramics Through Additives and Templating. *Journal of the American Ceramic Society* **2009**, *92* (7), 1534−1539.
(46) Gao, H. L.; Zhu, Y. B.; Mao, L. B.; Wang, F. C.; Luo, X. S.; Liu, Y. Y.; Lu, Y.; Pan, Z.; Ge, J.; Shen, W.; Zheng, Y. R.; Xu, L.; Wang, L. J.; Xu, W. H.; Wu, H. A.; Yu, S. H. Super-Elastic and Fatigue Resistant Carbon Material with Lamellar Multi-Arch Microstructure. *Nat. Commun.* **2016**, *7*, 12920−12927.
(47) Zhao, F.; Lin, L.; Zhang, J.; Liu, J.; Shi, J.; Godec, Y. Le; Courac, A. Ice-Templating: Integrative Ice Frozen Assembly to Tailor Pore Morphology of Energy Storage and Conversion Devices. *Adv. Mater. Technol.* **2023**, *8* (11), 2201968.
(48) Yoo, C. J.; Narayanan, P.; Jones, C. W. Self-Supported Branched Poly(Ethyleneimine) Materials for CO_2 Adsorption from Simulated Flue Gas. *J. Mater. Chem. A Mater.* **2019**, *7* (33), 19513−19521.
(49) Narayanan, P.; Lively, R. P.; Jones, C. W. Effect of SO_2 on the CO_2 Capture Performance of Self-Supported Branched Poly-(Ethyleneimine) Scaffolds. *Energy Fuels* **2023**, *37* (7), 5257−5269.
(50) Rim, G.; Priyadarshini, P.; Song, M.; Wang, Y.; Bai, A.; Realff, M. J.; Lively, R. P.; Jones, C. W. Support Pore Structure and Composition Strongly Influence the Direct Air Capture of CO_2 on Supported Amines. *J. Am. Chem. Soc.* **2023**, *145* (13), 7190−7204.
(51) Sakwa-Novak, M. A.; Jones, C. W. Steam Induced Structural Changes of a Poly(Ethylenimine) Impregnated γ-Alumina Sorbent for CO_2 Extraction from Ambient Air. *ACS Appl. Mater. Interfaces* **2014**, *6* (12), 9245−9255.
(52) Von Harpe, A.; Petersen, H.; Li, Y.; Kissel, T. Characterization of Commercially Available and Synthesized Polyethylenimines for Gene Delivery. *Journal of Controlled Release* **2000**, *69* (2), 309−322.
(53) Chaikittisilp, W.; Kim, H. J.; Jones, C. W. Mesoporous Alumina-Supported Amines as Potential Steam-Stable Adsorbents for Capturing CO_2 from Simulated Flue Gas and Ambient Air. *Energy Fuels* **2011**, *25* (11), 5528−5537.
(54) Ditmars, D. A.; Plint, C. A.; Shukla, R. C. Aluminum. I. Measurement of the Relative Enthalpy from 273 to 929 K and Derivation of Thermodynamic Functions for Al(s) from 0 K to Its Melting Point. *Int. J. Thermophys* **1985**, *6* (5), 499.
(55) Downie, D. B.; Martin, J. F. An Adiabatic Calorimeter for Heat-Capacity Measurements between 6 and 300 K. The Molar Heat Capacity of Aluminium. *J. Chem. Thermodyn* **1980**, *12* (8), 779−786.
(56) Thommes, M.; Kaneko, K.; Neimark, A. V.; Olivier, J. P.; Rodriguez-Reinoso, F.; Rouquerol, J.; Sing, K. S. W. Physisorption of Gases, with Special Reference to the Evaluation of Surface Area and Pore Size Distribution (IUPAC Technical Report). *Pure and Applied Chemistry* **2015**, *87* (9−10), 1051−1069.
(57) Walton, W. H. Feret's Statistical Diameter as a Measure of Particle Size. *Nature* **1948**, *162* (4113), 329−330.
(58) Haeri, M.; Haeri, M. ImageJ Plugin for Analysis of Porous Scaffolds Used in Tissue Engineering. *J. Open Res. Softw* **2015**, *3*, e1.
(59) Kirsebom, H.; Topgaard, D.; Galaev, I. Y.; Mattiasson, B. Modulating the Porosity of Cryogels by Influencing the Nonfrozen Liquid Phase through the Addition of Inert Solutes. *Langmuir* **2010**, *26* (17), 16129−16133.
(60) Crank, J. *The Mathematics of Diffusion*; Oxford University Press, 1979.
(61) Ruthven, D. M.; Loughlin, K. F. The Effect of Crystallite Shape and Size Distribution on Diffusion Measurements in Molecular Sieves. *Chem. Eng. Sci.* **1971**, *26* (5), 577−584.
(62) Moon, H. J.; Carrillo, J. M.; Leisen, J.; Sumpter, B. G.; Osti, N. C.; Tyagi, M.; Jones, C. W. Understanding the Impacts of Support-Polymer Interactions on the Dynamics of Poly(Ethyleneimine) Confined in Mesoporous SBA-15. *J. Am. Chem. Soc.* **2022**, *144* (26), 11664−11675.
(63) Kong, F.; Rim, G.; Song, M.; Rosu, C.; Priyadarshini, P.; Lively, R. P.; Realff, M. J.; Jones, C. W. Research Needs Targeting Direct Air Capture of Carbon Dioxide: Material & Process Performance Characteristics under Realistic Environmental Conditions. *Korean Journal of Chemical Engineering* **2022**, *39* (1), 1−19.
(64) Didas, S. A.; Sakwa-Novak, M. A.; Foo, G. S.; Sievers, C.; Jones, C. W. Effect of Amine Surface Coverage on the Co-Adsorption of CO_2 and Water: Spectral Deconvolution of Adsorbed Species. *J. Phys. Chem. Lett.* **2014**, *5* (23), 4194−4200.
(65) Bollini, P.; Didas, S. A.; Jones, C. W. Amine-Oxide Hybrid Materials for Acid Gas Separations. *J. Mater. Chem.* **2011**, *21* (39), 15100.
(66) Li, K.; Kress, J. D.; Mebane, D. S. The Mechanism of CO_2 Adsorption under Dry and Humid Conditions in Mesoporous Silica-Supported Amine Sorbents. *J. Phys. Chem. C* **2016**, *120* (41), 23683−23691.
(67) Hahn, M. W.; Steib, M.; Jentys, A.; Lercher, J. A. Mechanism and Kinetics of CO_2 Adsorption on Surface Bonded Amines. *J. Phys. Chem. C* **2015**, *119* (8), 4126−4135.
(68) Bacsik, Z.; Ahlsten, N.; Ziadi, A.; Zhao, G.; Garcia-Bennett, A. E.; Martín-Matute, B.; Hedin, N. Mechanisms and Kinetics for Sorption of CO_2 on Bicontinuous Mesoporous Silica Modified with N-Propylamine. *Langmuir* **2011**, *27* (17), 11118−11128.
(69) Lee, J. J.; Chen, C.-H.; Shimon, D.; Hayes, S. E.; Sievers, C.; Jones, C. W. Effect of Humidity on the CO_2 Adsorption of Tertiary Amine Grafted SBA-15. *J. Phys. Chem. C* **2017**, *121*, 23480.
(70) Bali, S.; Leisen, J.; Foo, G. S.; Sievers, C.; Jones, C. W. Aminosilanes Grafted to Basic Alumina as CO_2 Adsorbents—Role of Grafting Conditions on CO2 Adsorption Properties. *ChemSusChem* **2014**, *7* (11), 3145−3156.
(71) Castellazzi, P.; Notaro, M.; Busca, G.; Finocchio, E. CO_2 Capture by Functionalized Alumina Sorbents: DiEthanolAmine on γ-Alumina. *Microporous and Mesoporous Materials* **2016**, *226*, 444−453.
(72) Yu, J.; Chuang, S. S. C. The Structure of Adsorbed Species on Immobilized Amines in CO_2 Capture: An in Situ IR Study. *Energy Fuels* **2016**, *30* (9), 7579−7587.
(73) Yoo, C.-J.; Lee, L.-C.; Jones, C. W. Probing Intramolecular versus Intermolecular CO_2 Adsorption on Amine-Grafted SBA-15. *Langmuir* **2015**, *31* (49), 13350−13360.

https://doi.org/10.1021/cbe.3c00079
Chem Bio Eng. 2024, 1, 157−170